Dynamic Model of a Virtual Air Gap Reactor

David Sevsek ⬤, Marko Hinkkanen ⬤, *Fellow, IEEE,* Jarno Kukkola ⬤, and Matti Lehtonen ⬤

Abstract—**Variable reactors have been a vital component of power networks for decades, where they have been used as fault-current limiting devices or for reactive power compensation. Traditionally, modifying the inductance of predominantly mechanically operated variable reactors requires seconds to minutes. In contrast, virtual air gap (VAG) reactors can change the inductance within milliseconds, potentially improving power system stability. Existing dynamic models of VAG reactors cannot capture the entire system dynamics, limiting their applicability for simulations in the time-domain. This research presents two dynamic VAG reactor models, one with and one without core losses. The models capture all significant system dynamics using electromagnetic principles and VAG reactor flux linkage behavior. The proposed models were experimentally validated using a small VAG reactor. Over a broad operating range, both models accurately reproduce the dynamic behavior, transient response, and dominant harmonics of the small VAG reactor. Consequently, the models may be used for a variety of applications, such as time-domain simulations, harmonic analysis, and the development of suitable controllers for VAG reactors. In addition, engineers may use the core loss omitting model as a VAG reactor design tool, as the actual reactor is not required for modeling.**

Index Terms—**Dynamic model, finite element method (FEM), variable reactor, virtual air gap (VAG).**

I. INTRODUCTION

MODERN power distribution systems must be reliable, resilient against disturbances, and deliver high-quality power. Variable reactors have traditionally attenuated power quality issues and network disturbances such as voltage deviations or harmonics. Furthermore, they have been used to limit fault currents. Using technologies such as on-load tap-changers or variable air gap reactors, traditional variable reactors have the ability to change the inductance [1], [2]. Those systems have been valuable assets in the past. However, increasing power quality and safety requirements demand continuously adjustable reactors.

One method which has seen an increasing interest in recent years to attain continuous adjustability is the utilization of saturable reactors (SR) [3], [4]. SRs were described for the first time by Burgess in 1903 [5]. SRs utilize a second DC winding to create a DC-biased flux in a magnetic core, thereby changing

the magnetization of the SR. Hence, the DC current can regulate the reactor inductance smoothly and fast. The application of modern power electronics enables a precise DC current control improving inductance-changing speeds and accuracies of SRs. This enhancement can boost the power system stability. However, the lack of power electronics and the excessive costs limited the application of saturable reactors mainly to low-power applications in the last century.

Recently, there has been renewed interest in a novel class of SRs that rely on the virtual air gap (VAG) concept [6], [7], [8]. This novel class can be referred to as VAG reactors which became interesting due to the introduction of low-cost and high-power electronics and the commonly high durability of SRs. VAG reactors utilize pairs of secondary windings integrated into the magnetic core of the reactor. However, the winding direction of the secondary winding pairs is opposed. As a result, the DC currents flowing through the secondary windings create opposing DC fluxes. Hence, the secondary flux path closes locally, leading to a local saturation of the magnetic core. This local saturation phenomenon changes the magnetic reluctance of the core, influencing the primary winding flux linkage. Therefore, it can be concluded that the local core saturation via a DC current through immersed secondary control windings alters the inductance of the reactor. A straightforward real-time DC current controller that modifies the primary inductance of VAG reactors was presented in [7].

There have been several attempts to study VAG reactors [7], [8], [9], [10], [11], [12], [13], [14]. For instance, in [12], [13], a finite element analysis has been performed to determine the equivalent length of VAGs. However, only a few analytical modeling approaches enabling a dynamic performance investigation of VAG reactors have been presented in previous research [7], [9], [10], [14]. In [14], a design tool for VAG reactors was presented using reluctance networks. Similar to this, in [9], essential design features of VAG reactors, such as the core material and the dimensions of the VAG windows, have been investigated with the help of numerical magnetic field computations. Furthermore, in [10], a series of laboratory tests have been performed on a VAG reactor, demonstrating the voltage control capabilities of VAG reactors.

The only known study that developed a time-domain model concentrating on the dynamic behavior of VAG reactors was presented in [7]. This study presents a dynamic state-space model of a VAG reactor, validated with measurements of a low-voltage (LV) prototype. The time-domain modeling accuracy of the given model in [7] is acceptable. However, the model has a significant drawback. The state-space model fails to model the third harmonic. This weak spot comes from a
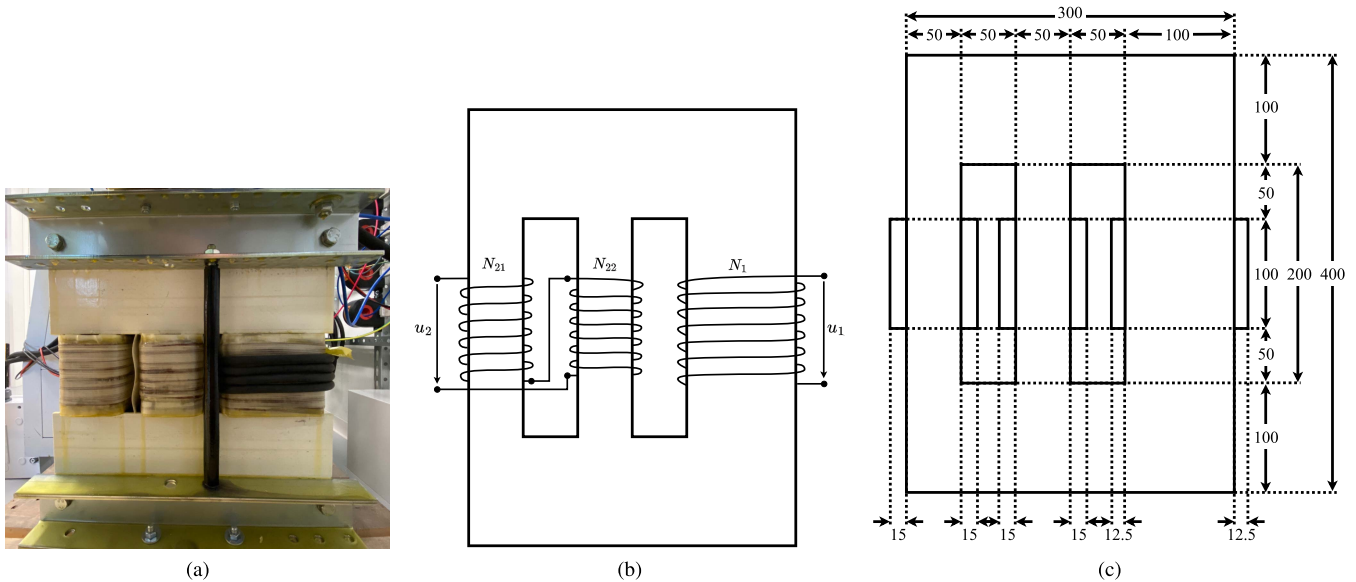
Fig. 1. VAG reactor: (a) Actual reactor. (b) Primary ($N_1 = 70$ turns) and secondary ($N_{21} = N_{22} = 99$ turns) coil configuration. (c) Dimensions in millimeters (Core depth $= 100$ mm).

simplification, assuming that the self-inductance of the primary winding depends solely on the DC control current, neglecting the influence of the primary current. This shortcoming reduces its usability when investigating the harmonic content of a VAG reactor and its inductance-changing capabilities.

This paper is an extension of work initially presented in [15]. The paper proposes two dynamic models for VAG reactors based on fundamental electromagnetic modeling principles [16], [17]. Both models reproduce the dynamic behavior of a VAG reactor with excellent accuracy, including the dominating harmonics. In its basic form, the dynamic model ignores the core losses. However, it is also shown that the core losses can be incorporated by augmenting the basic dynamic model with a simple core loss resistance as an enhancement compared to the nonlinear core loss resistance model in [15]. Finite element method (FEM) simulations of a VAG reactor produce current-flux-linkage mappings, which are the basis for the dynamic models. In addition, the accuracy of the proposed models is validated with a small VAG reactor that was not available in [15]. In addition to the work presented in [15], this paper presents the model characterization process and validates both models, including harmonic and transient analysis.

The proposed models are intended for use in time-domain simulations.

II. FEM MODEL

A. VAG Reactor

To verify the dynamic models described in this paper, a small VAG reactor was constructed and tested. Based on the assumption that the magnetic core would behave like grain-oriented steel of type ET150-30, the reactor was designed as shown in Fig. 1(a). Fig. 1(b) depicts the primary and secondary windings and their corresponding connections. Fig. 1(c) depicts

TABLE I
RATINGS OF VAG REACTOR

Primary side			
Parameter	Value	Unit	Description
U_1	230	V	Max. voltage (RMS)
I_1	10	A	Max. current (RMS)
Secondary side			
Parameter	Value	Unit	Description
U_2	1500	V	Max. voltage (Peak)
I_2	6	A	Max. DC current (RMS)

the dimensions of the reactor, and Table I lists the nominal values of the VAG reactor. The difference between Fig. 1(a) and (c) is entirely due to the plastic cover shielding the core.

B. Modeling Procedure

A 3D FEM model was built and simulated in COMSOL based on the dimensions illustrated in Fig. 1. All windings consist of copper and have a cross-sectional area of 3.53 mm^2.

First, the magnetization characteristics were measured as described in Section II-B1. Alternatively, the magnetization characteristics could be obtained from the manufacturer of the core material. Afterward, the measured BH characteristics were extrapolated to ensure good modeling accuracy for overfluxed regions in the core caused by the secondary control windings. The extrapolation method is elaborated in Section II-B2.

1) Magnetization Characteristics: The magnetic properties of the core material that was or will be used to create a VAG reactor may often be found from its datasheet. If the magnetization characteristics are reliable, the approach described in this section may be redundant. In many situations, however, the steel production process and coil fabrication can significantly alter the material properties. After initial testing of the VAG reactor described in this article, it became clear that the same
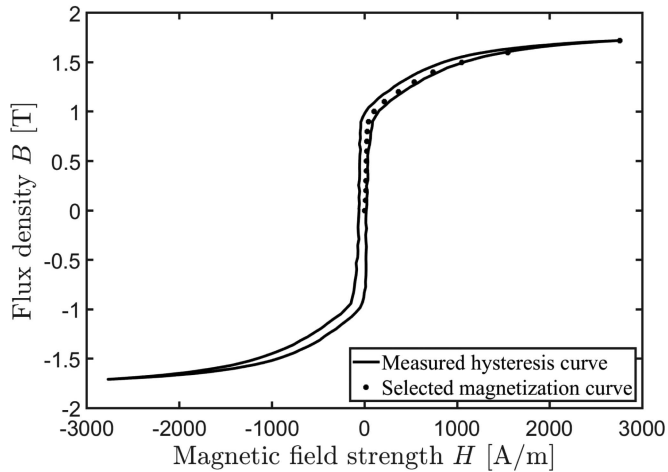
Fig. 2. Measured hysteresis curve of the VAG reactor and the derived magnetization curve.

Fig. 3. Measured and extrapolated magnetization characteristics of the VAG reactor core.

phenomena also occurred with the small VAG reactor. The mismatch between the desired and measured inductance was considerable. In such instances, the magnetization properties of the actual reactor must be measured.

The magnetization characteristics of the core can be determined by exciting the primary winding with a sinusoidal voltage, and the secondary windings are utilized to measure its induced voltage, similar to the procedure presented in [18], [19]. Therefore, the secondary windings have been reconnected so that the reactor works as a transformer. The magnetic flux density B in the core can then be estimated as

$$B = \frac{1}{N_2 A_c} \int u_2(t) dt, \tag{1}$$

where N_2 is the number of secondary windings, A_c is the cross-sectional area of the core, and u_2 is the induced voltage.

The magnetic field strength H can be determined as

$$H = \frac{N_1 i_1(t)}{l}, \tag{2}$$

where N_1 is the number of primary windings, i_1 is the measured current through the primary winding, and l is the mean path length of the core. In this case, the number of secondary windings is $N_2 = 99$. The effective cross-sectional area of the core is $A_c = 0.01$ m^2, and the mean path length of the core has been set to $l = 1$ m.

The integration of the measured voltage typically leads to an integration error due to measurement inaccuracies. This integration error has been removed by subtracting the mean of the measured voltage from the measurements. The resulting hysteresis curve is depicted in Fig. 2, which also illustrates the selected initial magnetization curve. The selected magnetization curve is approximately the median curve dissecting the measured hysteresis curve.

2) Extrapolation of Magnetization Characteristics: Datasheets of electrical steels and BH curve measurement techniques like the one described before typically provide data for magnetic flux densities up to 1.9 T. However, depending on the
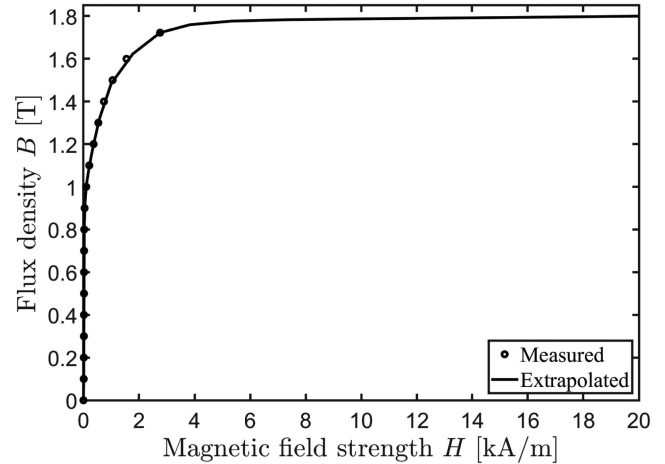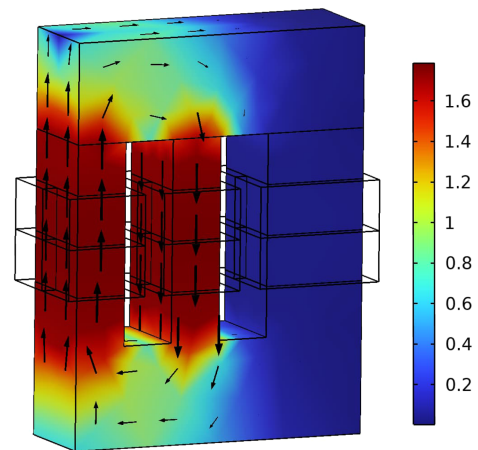

Fig. 4. Magnetic flux density in the core when the instantaneous primary voltage is at its peak and a high DC current flows through the secondary windings (FEM model).

design of the VAG reactor and the secondary control currents, overfluxed regions with flux densities above 1.9 T can occur.

Hence, it may be necessary to extrapolate the BH characteristics up to the magnetic saturation in some cases. In this study, the extrapolation was done with the help of COMSOL's built-in BH curve checker application, which extrapolates input data (i.e., the measured BH curve) up to magnetic saturation utilizing the Simultaneous Exponential Extrapolation (SEE) method, presented in [20]. The extrapolated BH curve of the studied VAG reactor created using the BH curve checker application can be seen in Fig. 3.

3) FEM Simulation: Based on the extrapolated magnetization characteristics and the dimensions of the VAG reactor, time-domain simulations in COMSOL were executed. Fig. 4 illustrates a case where the local saturation phenomena caused by the secondary DC current can be seen.

The current-flux-linkage mappings containing the necessary data for the dynamic models presented in this study can be created by performing FEM time-domain simulations at different
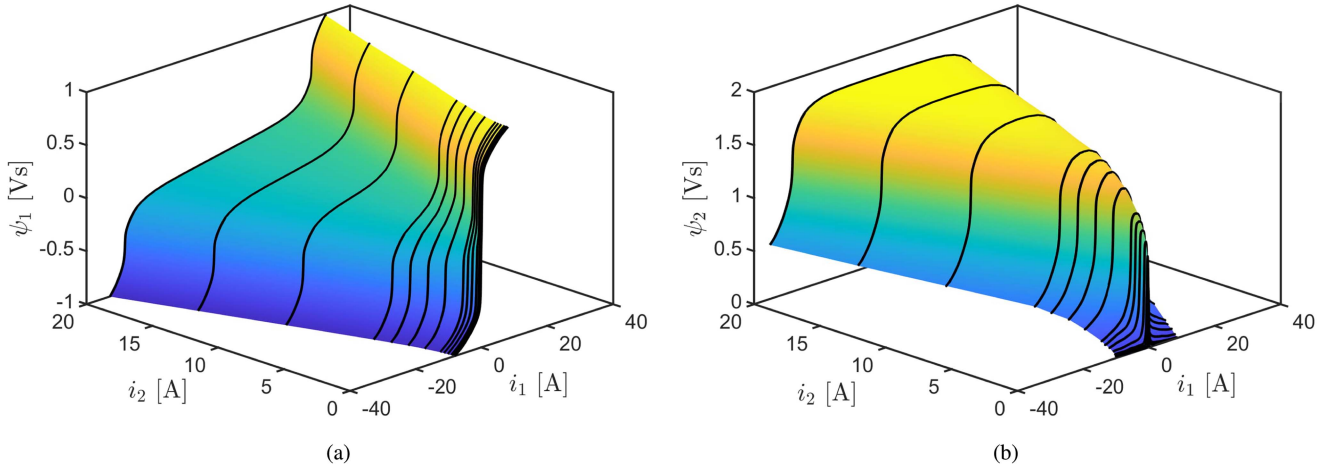
Fig. 5. Simulated flux linkage characteristics of the VAG reactor (FEM model). (a) $\psi_1(i_1, i_2)$. (b) $\psi_2(i_1, i_2)$.

operating points of the VAG reactor. Different operating points mean performing simulations with different secondary currents.

However, when performing the simulations, it is essential to remember that the rated operating flux density, the maximum flux linkage, and the primary voltage level are directly related. Therefore, performing all simulations at the rated primary voltage is essential. As a result, the current-flux-linkage mappings contain data at the rated operating flux density of the VAG reactor. For example, the flux linkage characteristics of the simulated VAG reactor in this study are shown in Fig. 5.

III. PROPOSED DYNAMIC MODELS

A. Dynamic Model

Generally, the voltage applied to a winding must balance the voltage drop in the winding resistance and the induced voltage. VAG reactors consist of primary and pairs of series-connected secondary windings. Hence, a dynamic model can be defined as

$$\frac{d\psi_1}{dt} = u_1 - R_1 i_1$$

$$\frac{d\psi_2}{dt} = u_2 - R_2 i_2, \tag{3}$$

where ψ_1 and ψ_2 represent the primary and secondary flux linkages, respectively. Furthermore, R_1 and R_2 depict the primary and secondary winding resistances, and u_1 and u_2 are the voltages over the primary and secondary windings, respectively. The primary i_1 and secondary i_2 currents are interconnected through the flux linkages as

$$i_1 = i_1(\psi_1, \psi_2)$$

$$i_2 = i_2(\psi_1, \psi_2). \tag{4}$$

On the basis of (3) and (4), a dynamic model of a VAG reactor can be constructed, excluding the core and other loss components, such as eddy-current-induced losses in the tank walls of oil-immersed VAG reactors. Fig. 6 illustrates the primary side of this dynamic model. The information about the flux linkages
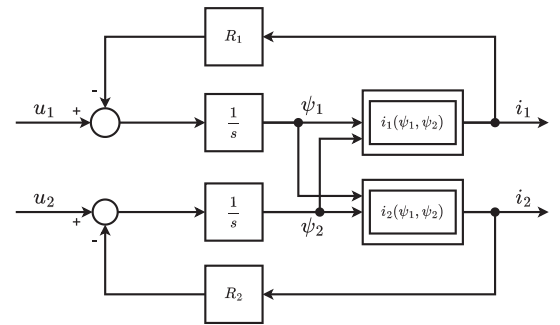
Fig. 6. Schematic representation of the dynamic model.
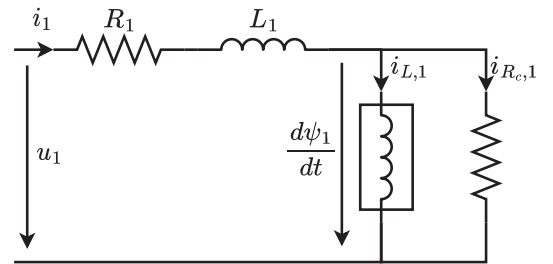
Fig. 7. Equivalent circuit of the nonlinear VAG reactor inductance and the parallel core-loss resistance augmented with a series inductance (primary side).

in (4) can also be understood as a set of nonlinear primary and secondary inductances.

B. Augmented Dynamic Model

The core losses can be considered by adding a constant parallel resistance to the nonlinear inductances. The augmentation of this parallel circuit with a series inductance simplifies the implementation and ensures a stable simulation of the augmented dynamic model. An equivalent circuit of the primary side of the augmented model can be seen in Fig. 7, and the schematic

Fig. 8. Schematic representation of the augmented model incorporating a constant core-loss resistance.

Fig. 9. Exemplary primary $u_{1,meas}$ and secondary $u_{2,meas}$ voltage measurement results from the VAG reactor, which can be utilized as an input file for a time-domain simulation of the dynamic models.
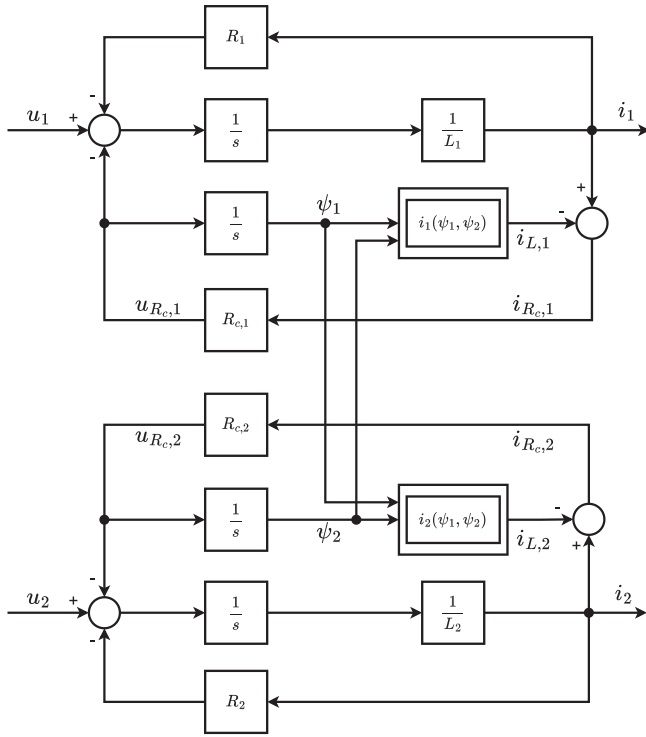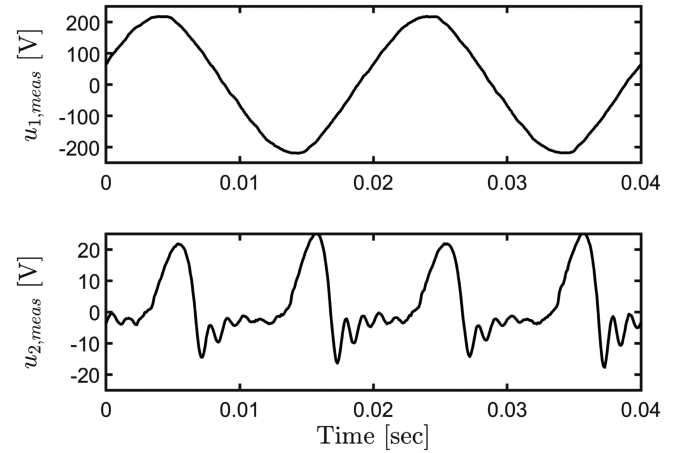
representation of the complete augmented model is shown in Fig. 8.

The dynamic models are similar to those of induction machines. However, in contrast to induction machine models, where all values are usually assumed to be constants, dynamic VAG reactor models include nonlinear inductances that are specified by knowledge about the flux linkages in the reactor as in (4). Furthermore, both dynamic models can simulate comparable devices with two pairs of windings in this configuration. However, the model might be expanded to include more windings. Nevertheless, this would enhance the modeling complexity and is outside the scope of this study.

IV. MODEL CHARACTERIZATION

A. Series Resistance

The series resistances of the primary R_1 and secondary R_2 windings are determined by injecting a constant DC current into the windings. The injected currents cause a voltage drop across the respective windings. After measuring the voltage drop, the winding resistance can be calculated using Ohm's law. This operation must be carried out on the real VAG reactor. However, if the dynamic model is to be utilized for design reasons (i.e. the VAG reactor has not yet been built), normal FEM software can be used to obtain resistance values.

B. Series Inductance

Depending on the design and ratings of the VAG reactor, the series inductances could be used as leakage inductances to model

stray fluxes. At higher currents, the magnetic field strength increases, and stray fluxes can induce significant eddy-current losses, for example, in tank walls of oil-immersed reactors. In this case, the current-flux-linkage mappings (see Section IV-D) could be divided into a magnetizing and a stray flux linkage portion, potentially leading to an increased modeling accuracy.

This paper avoids the division of flux linkages into magnetizing and leakage flux due to the missing tank wall in the studied VAG reactor and the low rated currents of the reactor. Hence, the series inductance solely serves as an insignificantly small parasitic inductance that enables the addition of the core resistance without creating direct feedthrough in the model. Hence, no parameterization is required on the reactor or the FEM program.

C. Core Resistance

In order to determine the constant core-loss resistances $Rc, 1$ and $Rc, 2$, an experiment must be conducted on the actual VAG reactor. Section V-A describes the experimental setup used to acquire measurement data for the parameterization procedure. The core-loss resistances of the VAG reactor can be determined with a single experiment. Therefore, any primary voltage level will be applied to the primary winding, and a power source will supply the secondary winding. In this study, the secondary winding was powered by a constant-current-controlling power source. The main objective of the experiment is to measure the primary $u1, meas$ and secondary $u2, meas$ voltages. The measured voltages serve as voltage input files for the augmented model. Fig. 9 illustrates the input file utilized in this study. This file enables the simulation of the augmented model with measured voltages in the time-domain. The simulation provides sets of primary and secondary current files, which are compared to the actual currents observed on the VAG reactor.

The goal is to select the core resistances to minimize the magnitude of the error between the simulated and measured currents. Thus, an objective function was defined as the sum of

TABLE II
VAG REACTOR MODEL PARAMETERS

Primary side			
Parameter	Value	Unit	Description
R_1	0.17	Ω	Winding resistance
$R_{c,1}$	272	Ω	Core-loss resistance
L_1	0.01	mH	Series inductance
Secondary side			
Parameter	Value	Unit	Description
R_2	0.39	Ω	Winding resistance
$R_{c,2}$	45	Ω	Core-loss resistance
L_2	0.01	mH	Series inductance

TABLE III
TEST NETWORK PARAMETERS

Parameter	Value	Unit	Description
$E_{1,2,3}$	230	V	Phase voltage
R_f	100	Ω	Fault resistance
C_{un}	4	μF	Artificial capacitive unbalance
C_0	8	μF	Zero-sequence capacitance
R_1	5.6	Ω	Line resistance
L_1	24	mH	Line inductance
R_{load}	80	Ω	Resistive load

squared residuals (SSR), and it is calculated as

$$\text{SSR} = \sum_{i=1}^{N} \left[\left(\frac{y_{i,1} - \widehat{y}_{i,1}}{\max(y_1)} \right)^2 + \left(\frac{|y_{i,1} - \widehat{y}_{i,1}|}{\max(y_1)} \right)^2 \right. \\ \left. + \left(\frac{y_{i,2} - \widehat{y}_{i,2}}{\max(y_2)} \right)^2 + \left(\frac{|y_{i,2} - \widehat{y}_{i,2}|}{\max(y_2)} \right)^2 \right],$$
(5)

where N represents the total number of measurement points. $y_{i,1}$ and $y_{i,2}$ stand for the ith measured primary and secondary current, while $\widehat{y}_{i,1}$ and $\widehat{y}_{i,2}$ are the respective simulated values. $\max(y_1)$ and $\max(y_2)$ are the measured maximum primary and secondary currents in the measurement interval utilized to normalize the error values.

Determining suitable values for the core resistances is an optimization task that can be challenging due to the potentially nonlinear and nonconvex nature of the problem. However, the objective function can be minimized by utilizing a genetic algorithm (GA). Therefore, the augmented model was constructed in MATLAB/Simulink, and the optimization was conducted utilizing the GA from MATLAB's global optimization toolbox. Table II illustrates the model parameters of both dynamic models, which were determined following the previously described methods.

D. Flux Linkage Characteristics

The essential data for both dynamic models, having the most significant influence on the modeling accuracy, is the information about the flux linkage characteristics of the VAG reactor to be studied. As defined in (4), the currents are functions of the respective flux linkages. The FEM simulations provide flux linkage characteristics which are functions of the respective currents as

$$\psi_1 = \psi_1(i_1, i_2)$$
$$\psi_2 = \psi_2(i_1, i_2).$$
(6)

A dataset for (4) can be attained by inverting those results. For instance, functions such as MATLAB's scatteredInterpolant, or griddedInterpolant create interpolants that act as look-up tables. Those interpolants perform linear interpolation on the datasets to provide the necessary information for the dynamic models.

V. RESULTS

Both dynamic models were experimentally validated with the help of the small VAG reactor. Therefore, time-domain MATLAB/Simulink models matching the models shown in Fig. 6 and Fig. 8 were created. As inputs for the Simulink models, experimentally recorded primary and secondary voltages from the small VAG reactor, comparable to those seen in Fig. 9, were utilized in the simulations. The model outputs, simulated primary and secondary currents, were then compared to the observed primary and secondary currents from the VAG reactor.

A. Experimental Setup

The VAG reactor was tested with two different experimental setups. Most of the tests were performed by directly connecting the primary side of the VAG reactor to a Teklab SM1603 isolation transformer. Thus, the VAG reactor could be tested at different primary voltage levels. Fig. 10 illustrates the test network used in the second step. The VAG reactor was functioning as an arc suppression coil (ASC) in this second step. That means the VAG reactor was connected to the neutral of the secondary side of the isolation transformer. The network resembles a single feeder in a distribution network with two separate line sections. The parameters of the network components are listed in Table III. The secondary side of the VAG reactor has been controlled with an EA-PSI 91500-30 laboratory power supply in constant current control mode. Different operating points of the VAG reactor have been investigated by selecting different DC secondary currents.

A LeCroy HVD3206 A, high voltage differential probe, was used to measure the primary voltage. The primary current was measured utilizing a LeCroy CP150 current probe. The secondary voltage was measured with a Testec TT-SI 9010 A differential probe, and the secondary current was measured utilizing a LeCroy AP015 current probe. A digital oscilloscope (LeCroy HDO6054) visualized and stored all measurements with a sampling frequency of 10 kHz for all measurements (i.e., voltages and currents).

B. Time-Domain Analysis

The time-domain simulation and measurement results were compared as a first model verification step. The high modeling accuracy of both dynamic models (i.e., dynamic and augmented dynamic) can be seen by comparing the simulated with the measured primary i_1 and secondary i_2 currents. Fig. 11 illustrates the behavior of the simulated models and the VAG reactor at a primary voltage of 150 V and an RMS secondary current of
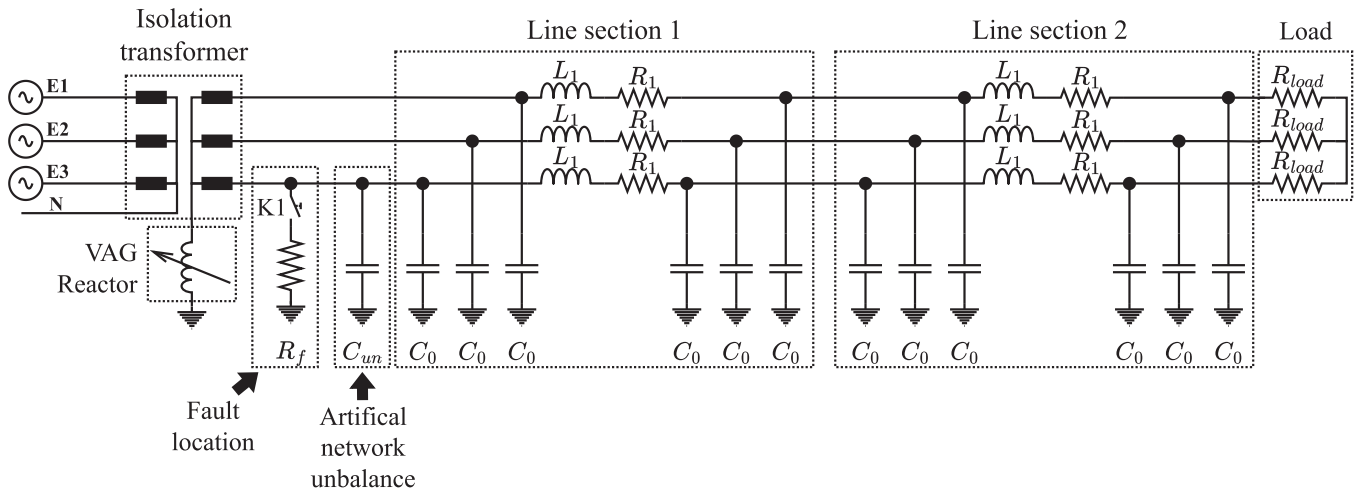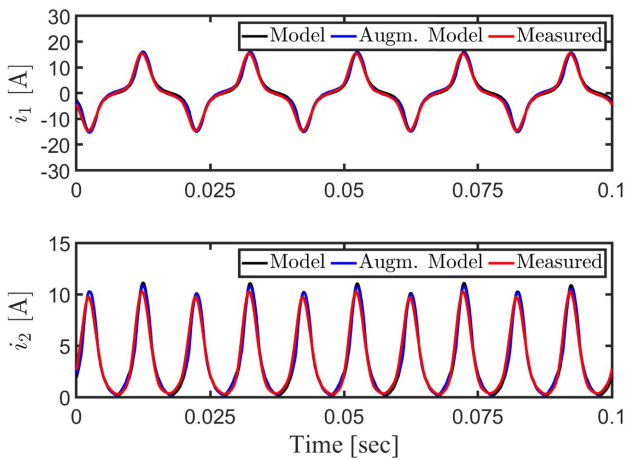
Fig. 10. Representation of the test network.

Fig. 11. Dynamic response of the VAG reactor and the dynamic models at a primary voltage level of 150 V (RMS) and a secondary current of 5 A (RMS).

approximately 5 A. It can be seen that both models perform equally well. Furthermore, both models match the measured currents almost perfectly. The minor difference between the simulated and the measured values could be caused due to measurement inaccuracies (i.e., the accuracy of current and differential probes).

Even though the power supply operates in the constant current control mode, a double-frequency component may be seen in the control current, as illustrated in Fig. 11. This double-frequency component is the result of the interaction between the AC flux and the flux created by the secondary windings. As the AC flux increases, it will partially reduce the flux density in the vicinity of the secondary windings because it opposes a portion of the flux produced by the secondary windings. When the AC flux again decreases, the flux density in this region returns to its initial value. This occurrence takes place when the AC flux density reaches the positive and negative peaks. Consequently, the secondary flux linkage experiences a double-frequency component, yielding a double-frequency AC component in the secondary

current. The magnitude of this AC component grows as the voltage across the primary side of the reactor rises, resulting in greater AC flux densities and more considerable variations in the local flux density around the secondary winding.

In addition to investigating the dynamic modeling accuracy when the RMS primary voltage and secondary currents are constant, it is essential to evaluate the modeling accuracy of both models during transient occurrences. The VAG reactor has thus been deployed as an ASC as part of the small test network illustrated in Fig. 10. By closing switch K1 in the test network, a resistance Rf representing a fault is connected to the test network. As demonstrated in Fig. 12, the fault causes the voltage across the primary winding (i.e., the neutral voltage of the network) and the current of the VAG reactor to increase after approximately 0.1 seconds suddenly. Furthermore, it can be seen that there are minor differences between the simulated and measured currents. Both models, however, exhibit the same transient behavior as the tested VAG reactor. The modeling accuracy difference between the dynamic model and the augmented dynamic model is negligible. Therefore, it may be stated that both dynamic models accurately reproduce the transient behavior of the VAG reactor.

Furthermore, because the augmentation of the dynamic model does not significantly increase the time-domain modeling accuracy, it can be avoided if the primary objective of the model is to resemble the inductive current production of a VAG reactor. VAG reactors are primarily inductors with typically small power factors. Hence, modeling core losses can be neglected in most cases. If that is the case, utilizing the dynamic model as a design tool for VAG reactors is possible. The non-augmented dynamic model does not necessarily require any characterization procedure performed on an actual VAG reactor. Instead, the series resistances can be approximated, and the flux linkage characteristics can be obtained from FEM simulations in case the magnetization behavior (i.e., BH curve) can be obtained from the steel manufacturer. That allows engineers to investigate a potential VAG reactor design without building it.
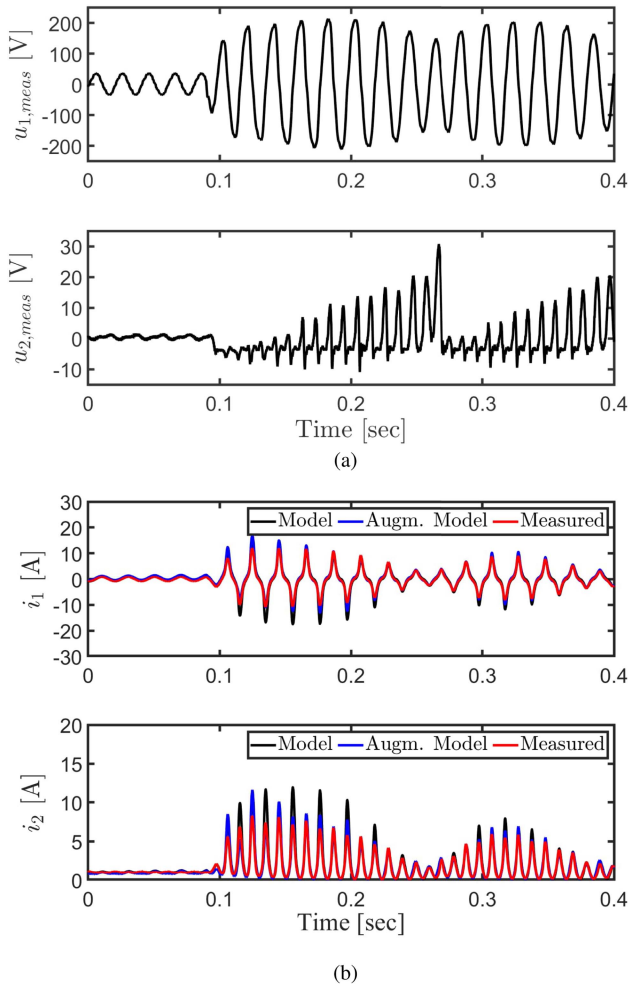
Fig. 12. Transient behavior of the VAG reactor. (a) Primary and secondary voltage measurements. (b) Measured and simulated primary and secondary currents.

However, this simplification is not necessarily valid for VAG reactors with higher shares of resistive current production, as demonstrated in [15]. If the simple core loss model in this study should not be sufficient, then it is possible to utilize a nonlinear core loss model which considers hysteresis and eddy current losses [21]. The implementation of this nonlinear model and its integration into the dynamic model has been previously described in [15].

C. Harmonic Analysis

The goals of the dynamic models include utilizing them for harmonic analysis and developing a controller that could mitigate the harmonics created by VAG reactors. Hence, the harmonic content in the primary current of the simulated dynamic model must resemble the actual VAG reactor closely. For instance, Fig. 13 illustrates the harmonic content in the primary current of the VAG reactor as a function of the secondary current at 230 V primary voltage. It can be seen that the harmonic content produced by both models agrees very well with the harmonic current production in the tested VAG reactor.
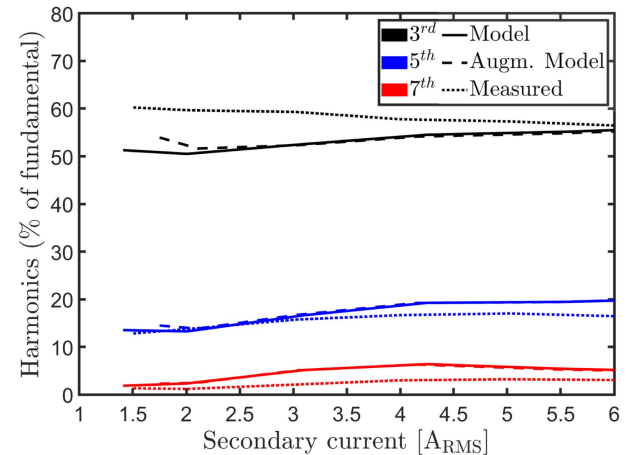

Fig. 13. Magnitude of different harmonic components in the primary current of the VAG reactor as a function of the secondary current. Simulated dynamic model (solid line), simulated augmented dynamic model (dashed line), and measured (dotted) results at rated nominal primary voltage (230 V).

D. Steady-State Analysis

The steady-state behavior of both dynamic models was compared to the measurement results of the actual VAG reactor as a last model verification step. Fig. 14 illustrates the difference between the simulated and the actual active and reactive power production of the primary side of the VAG reactor. It can be seen that the augmented model reduces the active power modeling error in contrast to the dynamic model. However, the reactive power production of both models is the same. In addition, Fig. 14(b) shows that both dynamic models model the reactive power output of the VAG reactor well. However, the reactive power production of the actual VAG reactor differs slightly from the modeled ones at a primary voltage level of 230 V. The discrepancy between the modeled and the actual reactive power production at 230 V can be explained by the inaccuracy of the magnetization characteristic measurements described in Section II-B1. The non-uniform shape of the reactor core increases the likelihood that the mean path length of the core differs from the chosen one. This has an impact on the calculated magnetic field strength. As a result, the hysteresis and magnetization curve, shown in Fig. 2, would change. Since inductance and inductive current production are directly linked to the magnetization curve, this is likely the source of the deviation between the measured and the simulated values. This deviation could be removed by either making a more accurate measurement of the magnetization curve or obtaining magnetization curve data from the steel manufacturer.

The primary inductance values of the VAG reactor, in Fig. 15, were calculated as

$$\text{Inductance} = \frac{U_1}{\omega I_{1,ind}}, \qquad (7)$$

where $\omega = 2\pi \cdot 50$ rad/s is the fundamental angular frequency of the primary voltage, U_1 and $I_{1,ind}$ are the primary RMS voltage and the RMS inductive primary current, respectively.
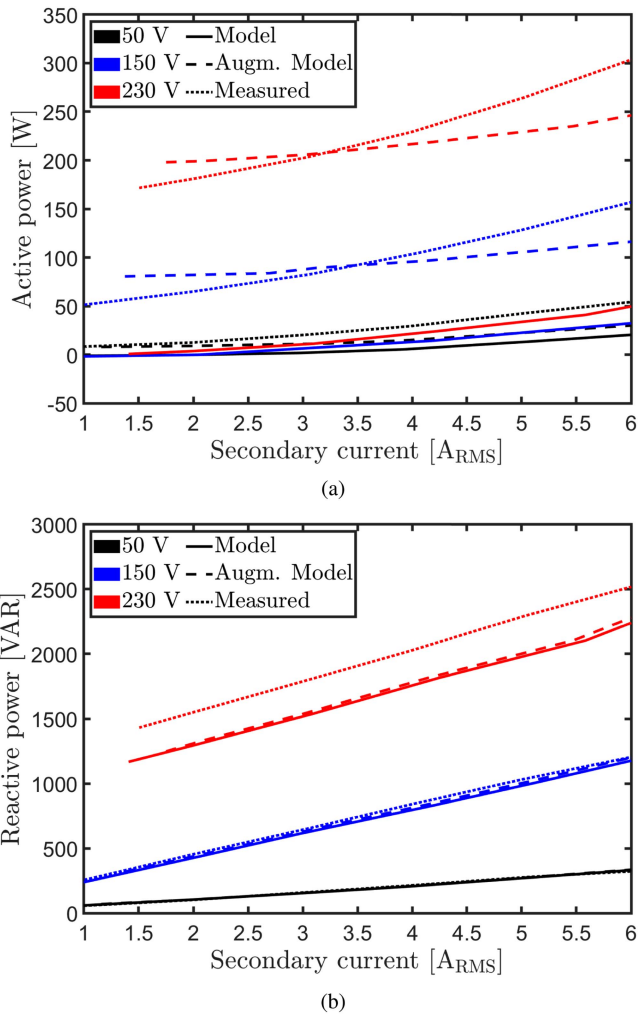
Fig. 14. (a) Active and (b) reactive power production of the VAG reactor as a function of the secondary current. Simulated dynamic model (solid line), simulated augmented dynamic model (dashed line), and measured (dotted) results at different primary voltage levels.
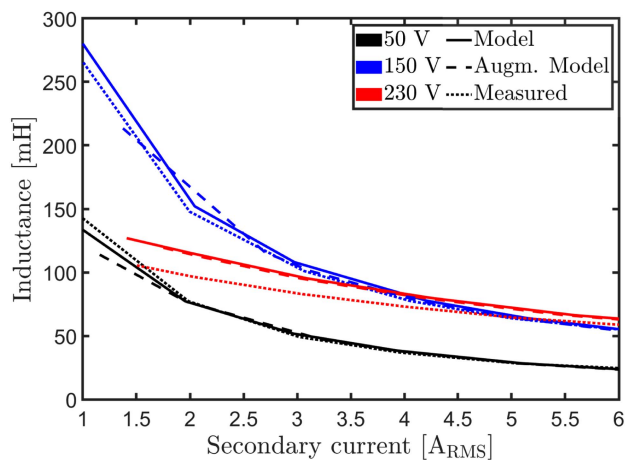

Fig. 15. Primary inductance of the VAG reactor as a function of the secondary current. Simulated dynamic model (solid line), simulated augmented dynamic model (dashed line), and measured (dotted) results at different primary voltage levels.

Fig. 15 shows that both dynamic models model the inductance of the VAG reactor well at 50 and 150 V. The deviation of the magnetization curve can also explain the slight difference between measurements and simulation models at 230 V.

It can be concluded that the results of both dynamic models, shown in Figs. 14 and 15, agree very well with the actual behavior of the VAG reactor over the whole range of secondary RMS control currents.

VI. CONCLUSION

Two dynamic models of a VAG reactor, including the essential system dynamics, have been developed. The model characterization approach for the proposed dynamic models has been explained in full, allowing the technique to be easily replicated for other VAG reactors. In addition, test results from a small VAG reactor have been compared to the developed models. This analysis revealed that both models accurately capture the dynamic response (time-domain and steady-state) of a VAG reactor across its entire operating range. These results indicate that both models may be utilized in time-domain simulations, such as simulations of power systems. Additionally, engineers may use the dynamic model to design VAG reactors. Future research should focus on developing a real-time controller for VAG reactors, which is facilitated by the models.

REFERENCES

[1] L. Yuan, X. Lei, l. Mengyue, Z. Shu, Z. Jingtao, and L. Mingxiang, "Small-disturbance line selection method applied to turn-adjusting arc suppression coil," in *Proc. IEEE 12th PES Asia-Pacific Power Energy Eng. Conf.*, 2020, pp. 1–5.

[2] K. Papp and R. Königi, "Arc suppression coils- The key component of modern earthfault protection systems," in *Proc. IEEE/PES Transmiss. Distrib. Conf. Expo.: Latin Amer.*, 2010, pp. 366–371.

[3] A. Dimitrovski, Z. Li, and B. Ozpineci, "Applications of saturable-core reactors (SCR) in power systems," in *Proc. IEEE PES T&D Conf. Expo.*, 2014, pp. 1–5.

[4] K. Mehmood, K. M. Cheema, M. F. Tahir, A. Saleem, and A. H. Milyani, "A comprehensive review on magnetically controllable reactor: Modelling, applications and future prospects," *Energy Rep.*, vol. 7, pp. 2354–2378, 2021. [Online]. Available: https://www.sciencedirect.com/science/article/pii/S2352484721002432

[5] C. F. Burgess and B. Frankenfield, "Regulation of electric circuits," U.S. Patent 720,884, 1903.

[6] J. Penttonen, "Magnetically controlled reactor - a novel component in smart grid," Ph.D. dissertation, Dept. Elect. Eng., Automat., Aalto Univ., Espoo, Finland, 2018.

[7] D. Dolan, "Modelling and performance evaluation of the virtual air gap variable reactor," Ph.D. dissertation, Dept. Elect. Comput. Eng., Univ. Toronto, Toronto, Ontario, Canada, 2009.

[8] V. Molcrette, J.-L. Kotny, J.-P. Swan, and J.-F. Brudny, "Reduction of inrush current in single-phase transformer using virtual air gap technique," *IEEE Trans. Magn.*, vol. 34, no. 4, pp. 1192–1194, Jul. 1998.

[9] E. Melgoza, J. Avila-Montes, and M. Madrigal, "Analysis of the magnetic characteristics of virtual-gap reactors," in *Proc. IEEE Int. Autumn Meeting Power Electron. Comput.*, 2013, pp. 1–6.

[10] J. Avila-Montes, D. Campos-Gaona, E. Melgoza Vázquez, and J. R. Rodríguez-Rodríguez, "A novel compensation scheme based on a virtual air gap variable reactor for AC voltage control," *IEEE Trans. Ind. Electron.*, vol. 61, no. 12, pp. 6547–6555, Dec. 2014.

[11] J. Avila-Montes and E. Melgoza, "Scaling the virtual air-gap principle to high voltage large power applications," in *Proc. IEEE 20th Int. Conf. Elect. Mach.*, 2012, pp. 757–762.

[12] S. Magdaleno and C. P. Rojas, "Control of the magnetizing characteristics of a toroidal core using virtual gap," in *Proc. IEEE Electron., Robot. Automot. Mechanics Conf.*, 2010, pp. 540–545.

[13] A. A. Abrishami and H. Heydari, "Improved accuracy for finite element modeling in virtual air gap lenght computation," in *Proc. IEEE 14th Int. Conf. Environ. Elect. Eng.*, 2014, pp. 271–274.

[14] J.-F. Brudny, G. Parent, and I. Naceur, "Characterization and modeling of a virtual air gap by means of a reluctance network," *IEEE Trans. Magn.*, vol. 53, no. 7, pp. 1–7, Jul. 2017.

[15] D. Sevsek, M. Hinkkanen, J. Kukkola, and M. Lehtonen, "Dynamic model of a virtual air gap variable reactor," in *Proc. IEEE PES Innov. Smart Grid Technol. Eur.*, Espoo, Finland, 2021, pp. 1–6.

[16] H. Woodson and J. Melcher, *Electromechanical Dynamics: Part I: Discrete Systems.* Hoboken, NJ, USA: Wiley, 1968.

[17] A. Fitzgerald, C. J. Kingsley, and S. D. Umans, *Electric Machinery*, 6th ed. New York, NY, USA: McGraw-Hill, 2003.

[18] V. Thottuvelil, T. Wilson, and H. Owen, "High-frequency measurement techniques for magnetic cores," *IEEE Trans. Power Electron.*, vol. 5, no. 1, pp. 41–53, Jan. 1990.

[19] S. Saeed, J. García, and R. Georgious, "Modeling of variable magnetic elements including hysteresis and eddy current losses," in *Proc. IEEE Appl. Power Electron. Conf. Expo.*, 2018, pp. 1750–1755.

[20] D. K. Rao and V. Kuptsov, "Effective use of magnetization data in the design of electric machines with overfluxed regions," *IEEE Trans. Magn.*, vol. 51, no. 7, pp. 1–9, Jul. 2015.

[21] M. Ranta, M. Hinkkanen, A. Belahcen, and J. Luomi, "Inclusion of hysteresis and eddy current losses in nonlinear time-domain inductance models," in *Proc. IEEE 37th Annu. Conf. Ind. Electron. Soc.*, 2011, pp. 1897–1902.

Marko Hinkkanen (Fellow, IEEE) received the M.Sc. (Eng.) and D.Sc. (Tech.) degrees in electrical engineering from the Helsinki University of Technology, Espoo, Finland, in 2000 and 2004, respectively. He is currently an Associate Professor with the School of Electrical Engineering, Aalto University, Espoo, Finland. His research interests include control systems, electric drives, and power converters. Dr. Hinkkanen was the co-recipient of the 2016 International Conference on Electrical Machines Brian J. Chalmers Best Paper Award, 2016 and 2018 IEEE Industry Applications Society Industrial Drives Committee Best Paper awards, and 2020 SEMIKRON Innovation Award. He is an Associate Editor of the IEEE TRANSACTIONS ON ENERGY CONVERSION and *IET Electric Power Applications*.

Jarno Kukkola received the B.Sc. (Tech.), M.Sc. (Tech.), and D.Sc. (Tech.) degrees in electrical engineering from Aalto University, Espoo, Finland, in 2010, 2012, and 2017, respectively. He is currently a Postdoctoral Researcher with the School of Electrical Engineering, Aalto University, Espoo, Finland. His research interests include control systems and grid-connected converters.

Matti Lehtonen received the master's and Licentiate degrees in electrical engineering from the Helsinki University of Technology, Espoo, Finland, in 1984 and 1989, respectively, and the D.Tech. degree from the Tampere University of Technology, Tampere, Finland, in 1992. From 1987 to 2003, he was with VTT Energy, Espoo, Finland, and has been a Professor with the Helsinki University of Technology since 1999. He is currently with Aalto University, Espoo, Finland, where he is currently the Head of power systems and high voltage engineering. His research interests include power system planning and asset management, power system protection, earth fault problems, harmonic-related issues, and information technology applications in distribution systems.

David Sevsek received the M.Sc. (Tech.) degree in advanced energy solutions in 2019 from Aalto University, Espoo, Finland, where he is currently working toward the Ph.D. (Tech.) degree. His research interests include power system protection and earth fault problems.